Interface Defects in C-face 4H-SiC MOSFETs: An Electrically-Detected-Magnetic-Resonance Study

T. Umeda[a], M. Okamoto[b], H. Yoshioka[b], G.-W. Kim[a], S. Ma[a], R. Arai[a], T. Makino[c], T. Ohshima[c], and S. Harada[b]

[a] Institute of Applied Physics, University of Tsukuba, Tsukuba 305-8573, Japan
[b] National Institute of Advanced Industrial Science and Technology (AIST), Tsukuba 305-8568, Japan
[c] National Institute for Quantum and Radiological Science and Technology (QST), Takasaki 370-1292, Japan

Using electrically-detected-magnetic-resonance spectroscopy and a device simulation, we studied dominant interface defects, named "C-face defects," in C-face 4H-SiC metal-oxide-semiconductor field-effect transistors (MOSFETs). The C-face defects act as hole traps via their donor levels, when they are not passivated by hydrogen atoms. The densities of unpassivated C-face defects were estimated to be from 4×10^{12} cm^{-2} to 13×10^{12} cm^{-2} in various C-face MOSFETs, which correlated with negative threshold-voltage (V_{th}) shifts. We explained influences of the C-face defects on the V_{th} instability and the channel mobility of C-face MOSFETs.

C-face 4H-SiC MOSFETs

Silicon carbide metal-oxide-semiconductor field-effect transistors (SiC-MOSFETs) are promising for low-energy-loss and high-power-density power transistors. SiC-MOSFETs are usually fabricated using a 4H-SiC(0001) ("Si face") surface to ensure a stability in their threshold voltages (V_{th}) (1,2). In contrast, a 4H-SiC($000\bar{1}$) ("C face") surface exhibits a wider range of the V_{th} instability (2,3), although C-face MOSFETs can achieve a much higher field-effect mobility (μ_{FE} = 60–100 cm^{2}V^{-1}s^{-1}) than the standard Si-face MOSFETs (μ_{FE} = 20–30 cm^{2}V^{-1}s^{-1}) (1-4). Figure 1 shows a typical example of the V_{th} instability observed in C-face MOSFETs. In MOSFET (a) which we call "bad type," the drain-current (I_d) versus gate-voltage (V_g) curve is horizontally shifted toward the negative direction after applying a negative V_g stress (-30 V) for 1800 sec. On the contrary, in MOSFET (b) or "good type," the negative V_{th} shift is drastically reduced even against a much longer stress time (20480 sec). However, the microscopic origin of such V_{th} instability as well as microscopic differences between C-face and Si-face MOS interfaces is still unclear.

In this paper, we present an electrically-detected-magnetic-resonance (EDMR) and device-simulation study on C-face MOSFETs. EDMR spectroscopy detected a large number of hole traps at the C-face MOS interface, which we have named the "C-face defects" (2,5). They were only observed on oxidized C face, and deeply connect with the characteristic properties of C-face MOSFETs. For instance, a primary difference in the samples shown in Figs. 1(a) and (b) was found in the densities of the C-face defects. We also found that their densities correlated with the negative V_{th} shifts in C-face MOSFETs. Accordingly, we propose a microscopic model for the V_{th} instability that the C-face

defects are incorporated into the SiO_2 layer during the oxidation, generating the positive fixed charges in the gate oxide.

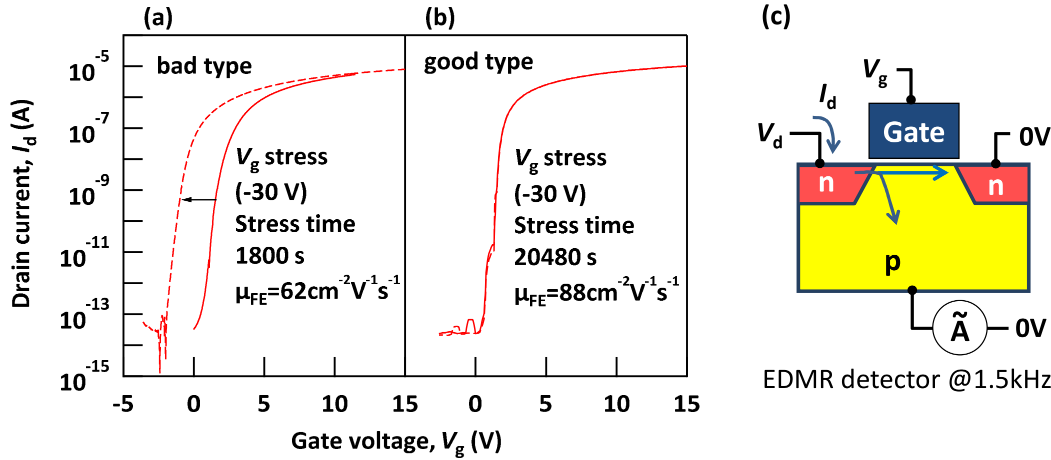

Figure 1. (a) and (b) I_d-V_g characteristics for C-face 4H-SiC MOSFETs (before γ-ray irradiation). Solid lines represent initial (un-stressed) curves, and dashed lines indicate the curves after a negative V_g stress. (c) I_d-V_g and EDMR setups. The drain voltage (V_d) was set to 0.1 V and -2.2 V for I_d-V_g and EDMR measurements, respectively. The source and well voltages were set to 0 V.

Experimental

C-face MOSFETs. Lateral *n*-channel C-face 4H-SiC MOSFETs (gate length = 100 μm, gate width = 150 μm) were prepared on a *p*-type epitaxial layer ([Al] ≈ 1×10^{16} cm^{-3}) of 4º-off 4H-SiC(000$\bar{1}$) wafers. A 50-nm-thick gate oxide was grown by *wet* oxidation at 1000ºC and was subjected to H_2 post oxidation anneal (POA) at 1100ºC for 30 min. The gate electrode was deposited on the gate oxide at room temperature for an Al electrode for "bad type" [Fig. 1(a)] and at 570ºC for a poly-Si electrode for "good type" [Fig. 1(b)]. This difference may relate to the difference shown in Fig. 1, however, we also suspect other factors, because we have seen a variation of both Al-gate and poly-Si-gate C-face MOSFETs. After the oxidation and POA, the process temperatures were kept to be lower than 570ºC, because high-temperature annealing (≥ 800ºC) is known to degrade the C-face MOSFETs (6).

Some of the MOSFETs were subjected to γ-ray irradiation causing the dissociation of hydrogen atoms from hydrogen-passivated defects. This effect is well known for the case of the P_b center at Si/SiO_2 interfaces (7). In a previous study (5), we found that the hydrogen-depassivation by γ-irradiation increased negative V_{th} shifts in C-face MOSFETs. Thus, the γ-irradiation enabled us to prepare a variety of C-face MOSFETs with a wide range of the V_{th} instability. We used γ-ray generated from ^{60}Co (average energy ≈ 1.4 MeV) and the dose was set to 0.5–40 Mrad. Our dose range was similar to that used for Si-MOS samples (7).

EDMR measurements. We carried out EDMR measurements at room temperature using a home-built EDMR spectrometer (2,5). In principle, EDMR can detect singly-occupied energy levels interacting with carriers. In such energy levels, the Pauli's principle permits spin-dependent carrier-capture processes, which lead to electron-spin-resonance (ESR)-induced current changes. Figure 1(c) shows our electrical setup. In the

EDMR mode, we used V_d = -2.2 V and monitored a drain-to-well current via the interface by an EDMR detector. Figure 2(a) shows actual current changes induced by the C-face defects. The current change is negative; ESR enhanced carrier-capture processes at the defects and reduced the current. EDMR spectroscopy amplified such a current change (generally, in ppm) under sweeping an external magnetic field, **B**, by using a lock-in amplifier synchronized to a magnetic-field modulation (we chose a modulation frequency of 1.5 kHz). ESR transitions were excited by microwave of 200 mW at 9.462 GHz.

EDMR observation on C-face defects (interfacial hole traps)

The C-face defects have *c*-axial g values of $g_{//}$ = 2.0016 and $g_{\perp}$ = 2.0023, which is revealed by an angular map shown in Fig. 2(b). This ESR signature is clearly different from the case of the Si-vacancy defect (g = 2.003, isotropic) observed in Si-face MOSFETs (8). Thus, we have to consider that different types of interface defects are formed at C-face and Si-face MOS interfaces, which should relate to opposite electrical properties between the two types of MOSFETs.

Figure 2(c) shows typical EDMR spectra of the two C-face MOSFETs examined in Fig. 1. As is seen in the figure, we could observe the same EDMR signals, which we have named “C-face defects” (2,5). The EDMR spectra include an isotropic doublet hyperfine (hf) splitting of 1.0 mT which is most probably due to a ^{1}H nuclear spin

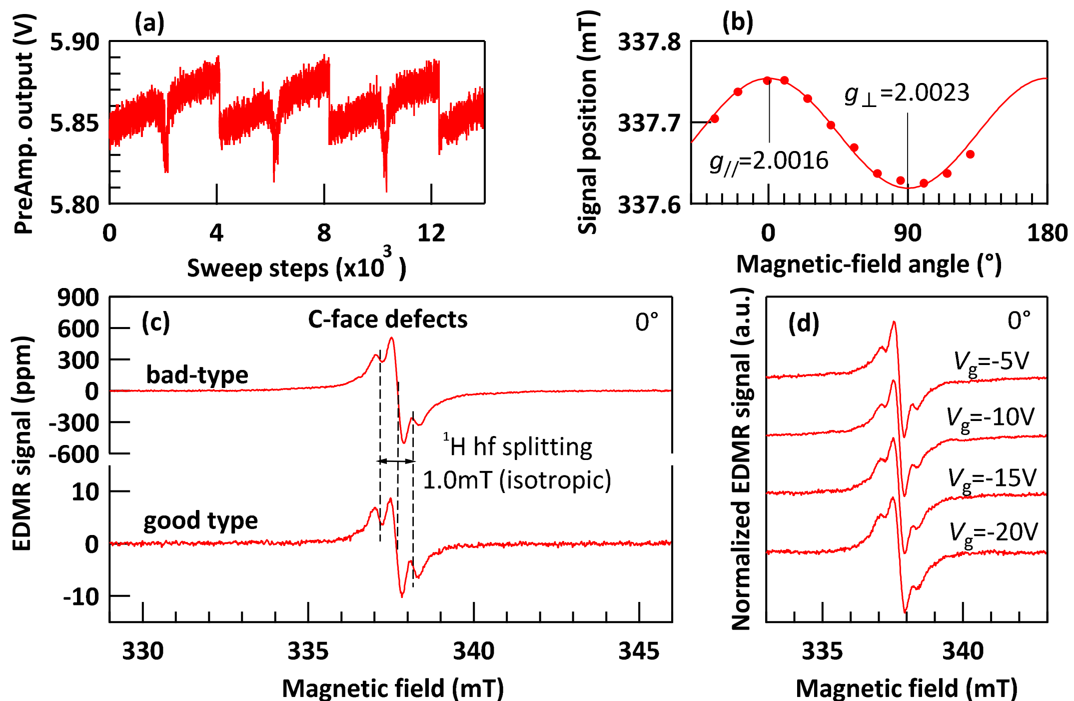

Figure 2. EDMR measurements on interfacial hole traps (named “C-face defects”) in C-face MOSFETs. (a) Example of ESR-induced current changes due to the C-face defects. Vertical axis is in proportion to a monitoring current. (b) Angular map of the C-face-defect signal. **B** parallels to $[000\bar{1}]$ and $[\bar{1}\bar{1}20]$ for 0º and 90º, respectively. (c) EDMR spectra measured using drain-to-well currents of -15 nA under V_g = -27 V and -10 V for the “bad-type” and “good-type” samples, respectively. (d) V_g dependence of EDMR spectra of C-face defects.

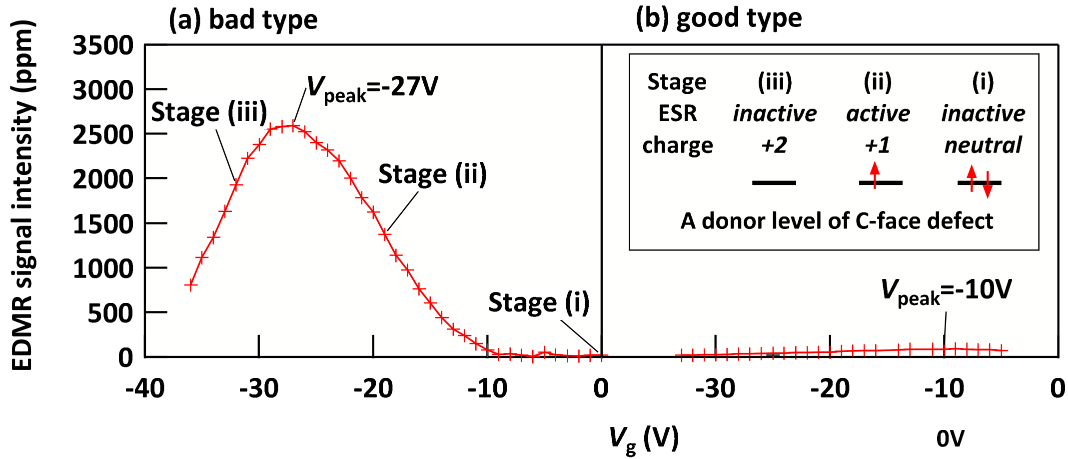

Figure 3. Gate-voltage dependences of EDMR signal intensities of the C-face defects. The signal intensities (peak-to-peak intensities) were measured for the same conditions as used for Fig. 2. MOSFETs were subjected to 4-Mrad γ-ray irradiation to enhance the EDMR signals by breaking hydrogen passivation of the C-face defects. The inset in (b) draws spin and charge states of a donor level of a C-face defect in association with the stages (i) to (iii).

(nuclear spin $I = 1/2$, natural abundance = 99.9%). This is not surprising because our C-face MOSFETs were subjected to wet oxidation and H_2 POA. Although the ratio of the ^{1}H hf signal and the central signal (without hf splitting) was found to be different between "bad type" and "good type," the largest difference between the two samples was their signal intensities, as is seen in the vertical axes of Fig. 2(c). The ratio of the hf and central signals was also changed with the V_g bias, as shown in Fig. 2(d).

The V_g dependences of peak-to-peak intensities of the C-face defects are examined in Figs. 3(a) and (b). In every sample, the C-face defects were observable only under a negative V_g, in other words, by supplying holes to the interface. The signal intensity increases with increasing a negative V_g, and reaches a peak at a certain V_g (we define it as V_{peak}) and turns into a decrease with a further negative V_g. These behaviors can be reasonably explained by a *donor level* of the C-face defect. As is shown in the inset of Fig. 3(b), the donor level exhibits three different charge and spin states. In the stage (i) [when $V_g \geq 0$ V, see Fig 3(a)], the donor level maintains a *doubly-occupied neutral* state, which is ESR-*inactive*. Thus, no EDMR signals appeared. In the stage (ii) (when $V_g < 0$ V), the donor level captured a hole, forming a *singly-occupied +1 charge* state, which is an ESR-*active* state. We therefore observed the EDMR signals. In the stage (iii), by further increasing negative V_g (or supplying excess holes), the formation of *empty +2 charge* states (ESR-*inactive*) has started. Then the EDMR signal intensity started to decrease. When returning V_g to 0 V, the EDMR signals immediately disappeared due to the emission of trapped holes. Obviously, the C-face defects behaved as interfacial hole traps.

As reported in our previous paper (5), the γ-ray irradiation drastically increased the EDMR signal of the C-face defects. This increase is caused by breaking the hydrogen passivation of the C-face defects. Similar hydrogen-depassivation phenomena were observed for interfacial dangling-bond centers such as the P_b centers (Si dangling bonds) at Si/SiO_2 interfaces (7) and the P_{bC} center (carbon dangling bonds) found in porous-SiC/SiO_2 interfaces (9). We, however, emphasize that each of the dangling bonds has an

acceptor level whose neutral state should be singly-occupied (ESR-active) (7,9,10). Such dangling bonds must become ESR-inactive when they are positively charged by hole trapping (10). Therefore, we should consider that the C-face defects are not the same type as the known dangling-bond centers. It is also notable that the doubly-occupied neutral donor levels of the C-face defects never capture electrons and never generate the Coulomb scattering of free carriers. Therefore, they have *no* influences on the channel mobility. This is consistent with the high channel mobility of C-face MOSFETs, in spite of the presence of the C-face defects.

Device simulation on donor levels of C-face defects

In the next place, we estimate the density of the active C-face defects, which are not passivated by hydrogen atoms, under the assumption that all the active C-face defects are converted into the singly-occupied +1 charge states at $V_g = V_{peak}$ (a starting point for the formation of +2 charge states). We performed a device simulation using a commercial device simulator (Sentaurus Device, Synopsys) (4), where the MOSFET structure is the same as that used in the experiments. Donor-type single-level interface states are introduced at E_T: neutral state for $E_T < E_F$ and +1 charge state for $E_F < E_T$. Because we cannot pinpoint E_T, it is assumed to be E_V + 0.5 eV (below E_F), which does not affect the estimation of the defect density. Under the same bias conditions as used in Fig. 3, we calculated E_F at the interface as a function of V_g with/without the donor levels [Fig. 4(a)]. At $V_g = 0$ V, E_F was calculated to be about E_V + 1.0 eV. Then, E_F moved toward E_V as V_g was negatively biased. For the case of the donor-level density (N_T) of 6×10^{12} cm^{-2}, E_F is pinned at the donor levels until they are fully positively charged at $V_g \approx -16$ V. Obviously, the negative V_g bias required for full charge of the donor levels (we define it V_{charge}) depends on N_T. We calculated a relationship between V_{charge} and N_T as shown in

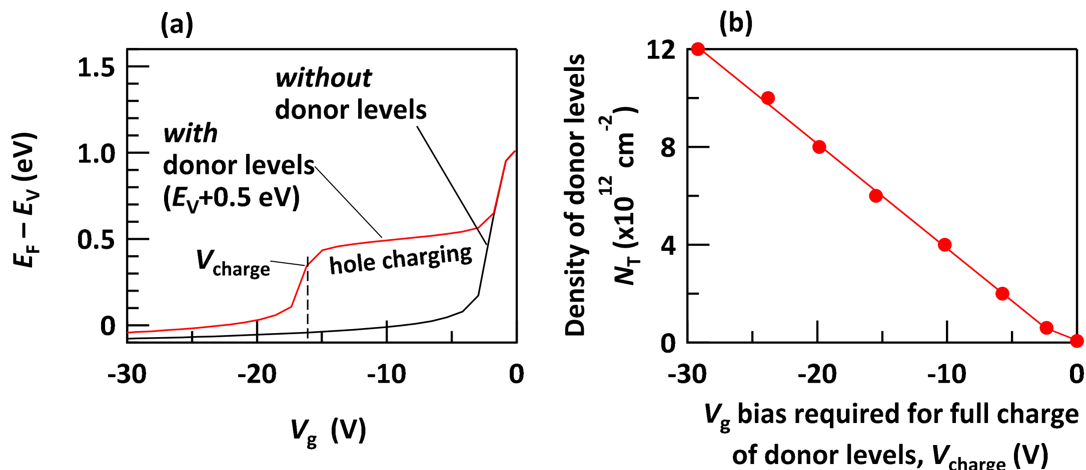

Figure. 4. Device simulations of a C-face 4H-SiC MOSFET including donor levels of the C-face defects. (a) Fermi level (E_F) at the drain edge of the C-face MOS interface as a function of V_g. The density of the donor levels (N_T) was assumed to be 6×10^{12} cm^{-2} at E_V + 0.5 eV. Until fully charging the donor levels with holes, $E_F - E_V$ is pinned at the donor-level position. (b) Simulation of a relationship between V_{charge} and N_T. Solid circles are obtained by the simulation.

Fig. 4(b). From this relation and an assumption that $V_{charge} \approx V_{peak}$, we estimated N_T to be 11×10^{12} cm^{-2} for V_{peak} = -27 V [Fig. 3(a)] and 3.9×10^{12} cm^{-2} for V_{peak} = -10 V [Fig. 3(b)].

Correlation between C-face defects and positive fixed charges

We prepared various C-face MOSFETs with different γ-ray irradiation, which revealed a wide range of the negative V_{th} shifts (5). Figure 5(a) summarizes a relationship between N_T (estimated from the procedure described in the preceding section) and the V_{th} shifts. As is seen in the figure, N_T seems to correlate with the negative V_{th} shifts which are caused by positive fixed charges in the gate oxide. To simply explain such a correlation, we suggest that the C-face defects are formed not only at the interface but also in the SiO_2 layer. When the oxidation is proceeding and a SiC/SiO_2 interface is going to the inner substrate, the C-face defects at the interface are possibly incorporated into the oxide, and partly remain as the source of positive fixed charges at there. This idea gives us a reason why C-face MOSFETs show large negative V_{th} shifts.

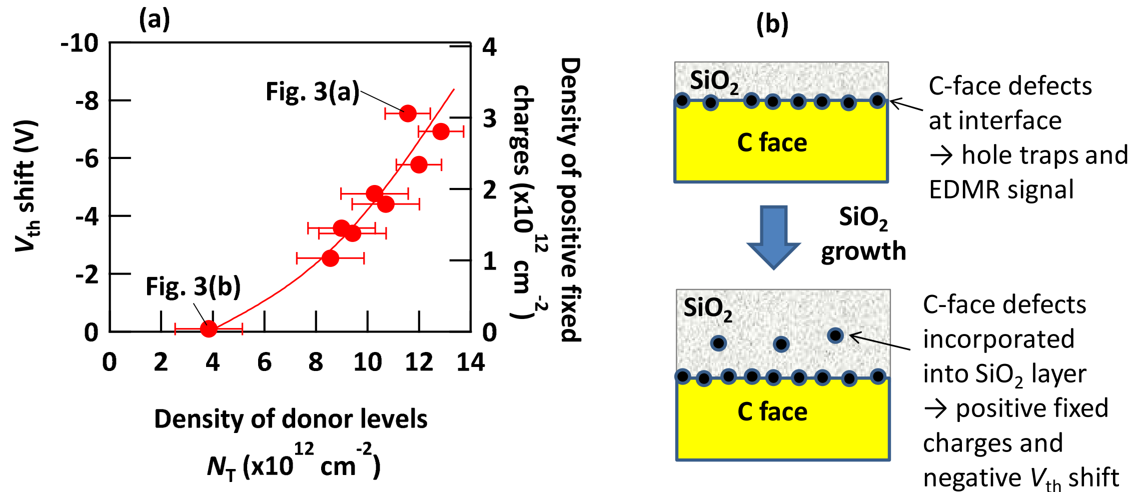

Figure 5. (a) Correlation between N_T and the negative V_{th} shifts in various C-face MOSFETs. The V_{th} shifts are saturated values measured after a long stress time; e.g., > 1500 sec and > 20000 sec for the samples used in Figs. 3(a) and (b), respectively. A solid curve is a guide for eyes. Horizontal error bars reflect uncertainties in V_{peak}. The right-hand-side axis represents the density of effective positive fixed charges calculated from the V_{th} shifts and the oxide capacitance. (b) A model of the C-face defects formed at the interface as well as in the oxide layer.

Summary

We have examined the dominant interface defects (the C-face defects) in C-face 4H-SiC MOSFETs. They acted as interfacial hole traps and closely related to the V_{th} instability of C-face MOSFETs, when they were not passivated by hydrogen atoms. Their densities were estimated to be from 4×10^{12} cm^{-2} to 13×10^{12} cm^{-2} in various C-face MOSFETs with a wide range of the negative V_{th} shifts. The whole EDMR results were understandable based on a deep donor level of the C-face defect. This level causes hole trapping under $V_g < 0$, while it does not affect the channel mobility under $V_g \geq 0$. We

found that the densities of the C-face defects are correlated with the negative V_{th} shifts or the densities of positive fixed charges in the oxide layer. Accordingly, we proposed that the C-face defects are partly incorporated into the oxide layer during the oxidation and become the source of the V_{th} instability. Although the microscopic origin of the C-face defects is still unidentified, their ESR signatures (axially-symmetric g values, ^{1}H hf splitting, spin-1/2 with a single positive charge state, etc.) will provide important hints for their identification.

Acknowledgments

This work was party supported by the JSPS KAKENHI grant No. 25286054 and 17H02781.

References

1. G. Y. Chung, C.C. Tin, J. R. Williams, K. McDonald, R.K. Chanana, R. A. Weller, M. Di Ventra, S. T. Pantelides, L. C. Feldman, O. W. Holland, M. K. Das and J. W. Palmour, *IEEE Elect. Dev. Lett.*, **22**, 176 (2001).
2. T. Umeda, M. Okamoto, R. Kosugi, R. Arai, Y. Sato, S. Harada, T. Makino and T. Ohshima, *ECS Trans.*, **58**(7), 55 (2013).
3. M. Okamoto, Y. Makifuchi, M. Iijima, Y. Sakai, N. Iwamuro, H. Kimura, K. Fukuda and H. Okumura, *Appl. Phys. Express*, **5**, 041302 (2012).
4. H. Yoshioka, J. Senzaki, A. Shimozato, Y. Tanaka and H. Okumura, *AIP Advances*, **5**, 017109 (2015).
5. G. W. Kim, R. Arai, S. J. Ma, M. Okamoto, H. Yoshioka, S. Harada, T. Makino, T. Ohshima and T. Umeda, *Mater. Sci. Forum*, **858**, 591 (2016).
6. S. Harada, M. Kato, T. Yatsuo, K. Fukuda and K. Arai, *Mater. Sci. Forum*, **600-603**, 675 (2009).
7. P. M. Lenahan and P. V. Dressendorfer, *J. Appl. Phys.*, **54**, 1457 (1983).
8. C. J. Cochrane, P. M. Lenahan and A. J. Lelis, *J. Appl. Phys.*, **109**, 014506 (2011).
9. J. L. Cantin, H. J. von Bardeleben, Y. Shishkin, Y. Ke, R. P. Devaty and W. J. Choyke, *Phys. Rev. Lett.*, **92**, 015502 (2004).
10. P. M. Lenahan and J. F. Conley, Jr., *J. Vac. Sci. Technol.*, B **16**, 2134 (1998).